Mathematical Biosciences 218 (2009) 40–49

Contents lists available at ScienceDirect

Mathematical Biosciences

journal homepage: www.elsevier.com/locate/mbs

Discontinuity induced bifurcations in a model of *Saccharomyces cerevisiae*

D.J.W. Simpson [a,*], D.S. Kompala [b], J.D. Meiss [a,1]

[a] Department of Applied Mathematics, University of Colorado, Boulder, CO 80309-0526, USA
[b] Department of Chemical Engineering, University of Colorado, Boulder, CO 80309-0424, USA

ARTICLE INFO

Article history:
Received 1 July 2008
Received in revised form 9 December 2008
Accepted 16 December 2008
Available online 27 December 2008

Keywords:
Piecewise-smooth systems
Andronov–Hopf bifurcations
Discontinuous bifurcations

ABSTRACT

We perform a bifurcation analysis of the mathematical model of Jones and Kompala [K.D. Jones, D.S. Kompala, Cybernetic model of the growth dynamics of *Saccharomyces cerevisiae* in batch and continuous cultures, J. Biotechnol. 71 (1999) 105–131]. Stable oscillations arise via Andronov–Hopf bifurcations and exist for intermediate values of the dilution rate as has been noted from experiments previously. A variety of discontinuity induced bifurcations arise from a lack of global differentiability. We identify and classify discontinuous bifurcations including several codimension-two scenarios. Bifurcation diagrams are explained by a general unfolding of these singularities.

1. Introduction

Yeasts are single-celled fungi of which more than 1000 different species have been identified. The most commonly used yeast is *Saccharomyces cerevisiae* which has been utilized for the production of bread, wine and beer for thousands of years. Biologists in a wide variety of fields use *S. cerevisiae* as a model organism.

A common experimental method for observing biochemical processes involved in yeast growth is that of continuous cultivation in a chemostat [1]. The cell growth takes place in a vessel that is continuously stirred. A nutrient containing fluid is pumped into the vessel and cell culture flows out of the vessel at the same rate, ensuring that the volume of culture in the reaction vessel remains constant. The rate of flow in and out divided by culture volume is called the *dilution rate*.

As a continuous culture experiment is carried out, it is common for the system to reach a steady state. At the steady state, the rate of cell division in the culture is equal to the dilution rate. However experimentalists in the late 1960s [2] observed that instead of settling to a steady state, continuous culture experiments of *S. cerevisiae* could in some cases produce stable oscillations. Von Meyenburg [3] discovered in subsequent experiments that these oscillations only occur in an intermediate range of values of the dilution rate (between about 0.08 h^{-1} and 0.22 h^{-1}). Concentrations of many chemicals have been found to oscillate along with cell number due to partial cell budding synchrony [4,5]. Much work has since been done to understand the cause of such oscillations, see for instance [6–8].

Saccharomyces cerevisiae has three metabolic pathways for glucose: fermentation, ethanol oxidation and glucose oxidation. The model of Jones and Kompala [9] hypothesizes that the competing metabolic pathways of the growing yeast cells create feedback responses that produce stable oscillations. It assumes that microorganisms will utilize the available substrates in a manner that maximizes their growth rate at all times. To enforce this optimization a 'maximum function' is introduced in the model equations; as a result, the model is an example of a piecewise-smooth, continuous dynamical system.

Piecewise-smooth systems are characterized by the presence of codimension-one phase-space boundaries, called *switching manifolds*, on which smoothness is lost. Such systems have been utilized in diverse fields to model non-smooth behavior, for example vibro-impacting systems and systems with friction [10–12], switching in electrical circuits [13–15], economics [16,17] and biology and physiology [18,19].

The interaction of invariant sets with switching manifolds often produces bifurcations that are forbidden in smooth systems. For instance, though period-doubling cascades are a common mechanism for the transition to chaos in smooth systems, in piecewise-smooth systems periodic orbits may undergo direct transitions to chaos [20,21]. These so-called *discontinuity induced bifurcations* can be non-smooth analogues of familiar smooth bifurcations or can be novel bifurcations and unique to piecewise-smooth systems. A bifurcation in the latter category that is simple in appearance (for example the transition from a stable period-1 solution to a stable period-3 solution in a piecewise-smooth map) often corresponds to a combination of a countable sequence of smooth bifurcations. In this situation, arguably, the piecewise-smooth system describes the dynamics more succinctly than any smooth system is able to. Alternatively bifurcations in piecewise-smooth systems

* Corresponding author.
E-mail address: simpson@colorado.edu (D.J.W. Simpson).
[1] Supported from the NSF under Grant DMS-0707659.

0025-5564/$ - see front matter © 2009 Elsevier Inc. All rights reserved.
doi:10.1016/j.mbs.2008.12.005

may be extremely complicated, see for instance [20,12,14] and references within.

A piecewise-smooth, continuous system is one that is everywhere continuous but non-differentiable on switching manifolds. In such a system, the collision of a mathematical equilibrium (i.e., steady state, abbreviated to equilibrium throughout this paper) with a switching manifold may give rise to a *discontinuous bifurcation*. As the equilibrium crosses the switching manifold, its associated eigenvalues generically change discontinuously. This may produce a stability change and bifurcation. In two-dimensional systems, all codimension-one discontinuous bifurcations have been classified [22], but in higher dimensions there are more allowable geometries and no general classification is known. See for instance [23,24] for recent investigations into three-dimensional systems.

In this paper we present an analysis of discontinuity induced bifurcations in the eight-dimensional *S. cerevisiae* model of Jones and Kompala [9]. The model equations are stated in Section 2. In Section 3 we illustrate a two-parameter bifurcation set indicating parameter values at which stable oscillations occur. The bifurcation set also shows curves corresponding to codimension-one discontinuous bifurcations. These bifurcations are analogous to saddle-node and Andronov–Hopf bifurcations in smooth systems. Bifurcations relating to stable oscillations are described in Section 4. We observe period-adding sequences over small regions in parameter space. In Section 5 we provide rigorous unfoldings of codimension-two scenarios seen in the bifurcation set from a general viewpoint. Finally Section 6 presents conclusions.

2. A model of the growth of *S. cerevisiae*

Jones and Kompala [9] give the following model equations:

$$
\begin{aligned}
\frac{dX}{dt} &= \left(\sum_i r_i v_i - D\right)X,\\
\frac{dG}{dt} &= (G_0 - G)D - \left(\tfrac{r_1 v_1}{Y_1} + \tfrac{r_3 v_3}{Y_3}\right)X - \phi_4\left(C\tfrac{dX}{dt} + X\tfrac{dC}{dt}\right),\\
\frac{dE}{dt} &= -DE + \left(\phi_1 \tfrac{r_1 v_1}{Y_1} - \tfrac{r_2 v_2}{Y_2}\right)X,\\
\frac{dO}{dt} &= k_L a(O^* - O) - \left(\phi_2 \tfrac{r_2 v_2}{Y_2} + \phi_3 \tfrac{r_3 v_3}{Y_3}\right)X,\\
\frac{de_1}{dt} &= \alpha u_1 \tfrac{G}{K_1+G} - \left(\sum_i r_i v_i + \beta\right)e_1 + \alpha^*,\\
\frac{de_2}{dt} &= \alpha u_2 \tfrac{E}{K_2+E} - \left(\sum_i r_i v_i + \beta\right)e_2 + \alpha^*,\\
\frac{de_3}{dt} &= \alpha u_3 \tfrac{G}{K_3+G} - \left(\sum_i r_i v_i + \beta\right)e_3 + \alpha^*,\\
\frac{dC}{dt} &= \gamma_3 r_3 v_3 - (\gamma_1 r_1 v_1 + \gamma_2 r_2 v_2)C - \left(\sum_i r_i v_i\right)C,
\end{aligned}
\tag{2.1}
$$

where X, G, E and O represent the concentrations of cell mass, glucose, ethanol (in g L^{-1}) and dissolved oxygen (in mg L^{-1}) in the culture volume, respectively. Each e_i represents the intracellular mass fraction of a key enzyme in the ith metabolic pathway. C represents the intracellular carbohydrate mass fraction. The subscripts 1, 2 and 3 correspond to the three pathways: fermentation, ethanol oxidation and glucose oxidation, respectively; r_i represents the growth rate on each pathway. Formulas for the growth rates and other functions are given in Appendix B. Details concerning the derivation of the model are found in [9] and expanded in the M.S. thesis of Jones [25].

In particular, the equation

$$
v_i = \frac{r_i}{\max(r_1, r_2, r_3)}, \tag{2.2}
$$

is introduced to model the regulation of enzyme activity by numerous biochemical mechanisms. Each v_i is a smooth function except at points where the two largest r_i are equal; at these points each v_i has discontinuous derivatives with respect to some of the variables. All eight differential equations have at least one term containing a v_i and thus display the same lack of smoothness properties. Therefore the model is a piecewise-smooth, continuous system. Our goal is to understand the effects that this non-smoothness has on the resulting dynamics.

This paper focuses on variations in values of two parameters, namely the dilution rate, D (in h^{-1}), and the dissolved oxygen mass transfer coefficient, $k_L a$ (in h^{-1}). Values for all other parameters are given in Appendix B and were kept constant throughout the investigations.

A key property of the system (2.1), is that the positive hyper-octant is forward invariant. That is, if the values of all variables are initially positive, they will remain positive for all time. This is, of course, a property that is required for any sensible model, since negative values of the variables are not physical. Furthermore, within the positive hyper-octant all trajectories are bounded forward in time. In other words, solutions always approach some attracting set which could be an equilibrium, a periodic orbit or a more complicated and possibly chaotic attractor.

3. A bifurcation set

In this section we describe a numerically computed bifurcation set for the system (2.1), see Fig. 1. We find a single, physically meaningful equilibrium (steady state) except in small windows of parameter space between saddle-node bifurcations. For small values of D, this equilibrium is stable. If we fix the value of $k_L a$ and increase D, the first bifurcation encountered is an Andronov–Hopf bifurcation (labeled HB_1 in Fig. 1). Slightly to the right of HB_1 the equilibrium is unstable and solutions approach a periodic orbit or complicated attractor (see Section 4). As the value of D is increased further a second Hopf bifurcation (HB_{2a} or HB_{2b}) is encountered that restores stability to the equilibrium (unless $k_L a \approx 230$, see below).

Recall, the system is piecewise-smooth, continuous as a result of a maximum function in the rate coefficient, (2.2). Since the switching manifold is codimension-one, it is a codimension-one phenomenon for the equilibrium to lie precisely on a switching manifold. Though an analytical formula for the equilibrium seems difficult to obtain, we have been able to numerically compute curves in two-dimensional parameter space along which this codimension-one situation occurs – the black curves in Fig. 1. We refer to these as *curves of discontinuity*. The curves of discontinuity divide parameter space into three regions where one of the r_i is larger than the other two, at the equilibrium. They may also correspond to discontinuous bifurcations, as described below. Physically, crossing a curve of discontinuity corresponds to a change in the preferred metabolic pathway at equilibrium.

Fig. 2 shows an enlargement of Fig. 1 near two points on a curve of discontinuity. In panel A, along the curve of discontinuity, below the point (a) and above the point (c), there is no bifurcation. Between (a) and (c), numerically we have observed that a periodic orbit is created when the equilibrium crosses the switching manifold. Between (a) and (b), the orbit is unstable and emanates to the right of the curve of discontinuity. Between (b) and (c) the orbit is stable and emanates to the left. We refer to these bifurcations as subcritical and supercritical *discontinuous Hopf bifurcations*, respectively. The codimension-two point (b), is akin to a Hopf bifurcation at which the constant determining criticality vanishes. We expect that a locus of saddle-node bifurcations will emanate from this point, in manner similar to that in smooth systems.

Two of the loci of smooth Hopf bifurcations, HB_{2a} and HB_{2b}, collide with the curve of discontinuity at (a) and (c). Near these points

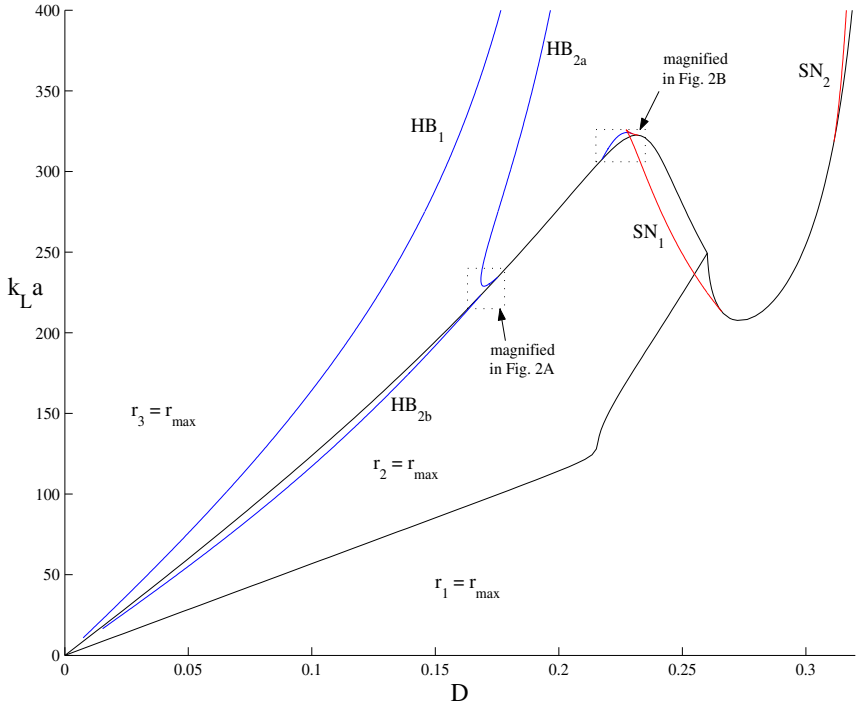

Fig. 1. A bifurcation set for the system (2.1). HB, Hopf bifurcation; SN, saddle-node bifurcation. The parameter space is divided into three regions within each of which a different metabolic pathway is preferred at equilibrium.

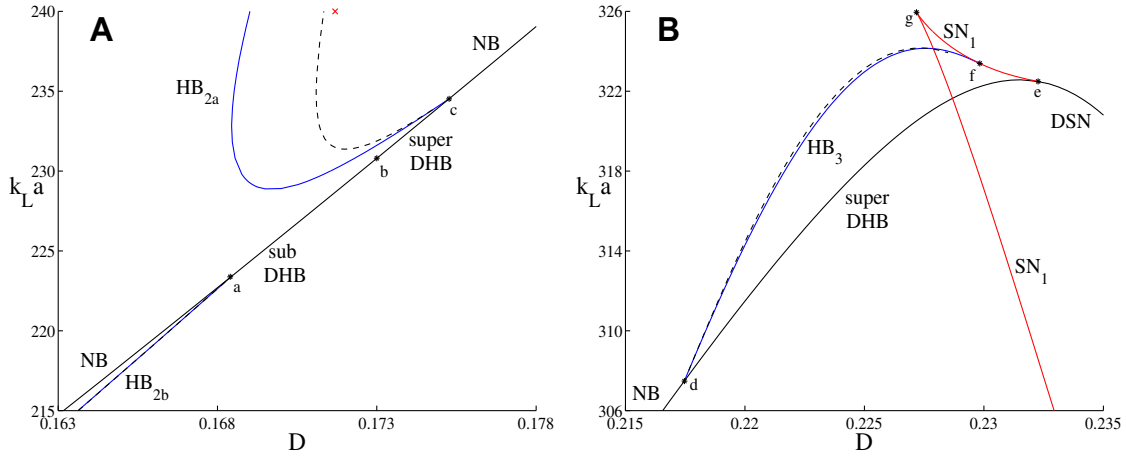

Fig. 2. Magnified views of Fig. 1. HB, Hopf bifurcation; SN, saddle-node bifurcation. The curves of discontinuity are labeled by their corresponding bifurcations: NB, no bifurcation; DHB, discontinuous Hopf bifurcation (with criticality indicated); DSN, discontinuous saddle-node bifurcation. The dashed curves correspond to the grazing of a Hopf cycle with a switching manifold. There are three such curves, these emanate from the points (a), (c) and (d) (note, the curve that emanates from (a) is barely distinguishable from HB_{2b}). In panel A, one point on a locus of saddle-node bifurcations of a Hopf cycle is shown with a red cross. (For interpretation of the references to color in this figure legend, the reader is referred to the web version of this article.)

these Hopf bifurcations are subcritical. Unstable periodic orbits emanate from the Hopf bifurcations and are initially of sufficiently small amplitude to not intersect a switching manifold. However, as we move away from the Hopf bifurcations, the amplitude of the Hopf cycles grow and they graze the switching manifold along the dashed curves in Fig. 2. No bifurcation occurs at the grazing because the system is continuous [26]. As we will show in Theorem 5.4, the grazing curves intersect the Hopf loci tangentially. The unstable cycles persist beyond grazing until they collide with a stable cycle in a saddle-node bifurcation. Loci of saddle-node bifurcations of periodic orbits are not shown in the figures because we have not been able to accurately numerically compute more than a single point (when $k_La = 240$, see Fig. 2A) on the curves due to the stiffness, non-smoothness and high dimensionality of the system (2.1). We expect one such curve to emanate from (c) and lie extremely close to the upper grazing curve as has recently been shown for two-dimensional systems [27].

Fig. 2B, shows a second magnification of Fig. 1 near $D = 0.225$ and $k_La = 320$. Loci of Hopf bifurcations and saddle-node bifurcations of the equilibrium have endpoints at (d) and (e) that lie on a curve of discontinuity. We will show in Section 5 that bifurcations and dynamical behavior in neighborhoods of (d) and (e) are predicted by Theorems 5.4 and 5.1, respectively. To the left of the point (d), no bifurcation occurs along the curve of discontinuity. To the right of (e), points on the curve of discontinuity act as saddle-node bifurcations, hence we refer to these as *discontinuous*

saddle-node bifurcations. From the point (d) to very close to (e), the curve of discontinuity corresponds to a supercritical discontinuous Hopf bifurcation. A Takens–Bogdanov bifurcation occurs at (f) where the Hopf locus, HB_3, terminates at the saddle-node locus, and the point (g) corresponds to a cusp bifurcation [28]. Near the points (e) and (f) we believe there are a variety of additional bifurcations that we have not yet identified. The system exhibits stable oscillations in the region between the smooth Hopf bifurcations and discontinuous Hopf bifurcations, but to our knowledge, oscillations in this parameter region have not been observed experimentally.

4. Simple and complicated stable oscillations

Experimentally observed oscillations match well with the model (2.1) in terms of the shapes of curves in time series plots, see [9]. In particular, time series plots of the variable most readily determined experimentally, the dissolved oxygen concentration, O, match almost exactly with model. The range of D values over which oscillations occur varies with k_La, as observed experimentally [4]. Similarly if the value of D is fixed and k_La is varied, sustained oscillations may arise or disappear, see [29]. Our bifurcation analysis reveals that oscillations occur for parameter values between HB_1 and HB_2 in Fig. 1, over a range of D values from 0.0 h^{-1} to approximately 0.2 h^{-1}, as typically observed in experimental data. In this section, we will discuss oscillatory dynamics predicted by the model in more detail.

Fig. 3 shows a one parameter bifurcation diagram of the system (2.1) when $k_La = 150$. The black [magenta] dots represent local maxima [minima] O on the stable oscillating cycle. For values of D between about 0.0927 and 0.1172, all three pathways are at some time preferred over one period of the solution, see Fig. 4. In particular, very soon after the preferred pathway changes from glucose oxidation to fermentation (green to cyan in Fig. 4), the concentration of dissolved oxygen rebounds slightly before continuing to decrease. Thus local maxima appear below the equilibrium value in Fig. 3. For larger values of D, still to the left of the rightmost Hopf bifurcation, fermentation is no longer a preferred pathway at any point on the stable solution, and the lower local maximum is lost. Also, the absolute maximum undergoes two cusp catastrophes at $D \approx 0.111,\ 0.117$.

Different values of k_La yield similar bifurcation diagrams, we show a collection in Fig. 5. As a general rule there is a rapid change from a stable equilibrium to a large amplitude orbit near the leftmost Hopf bifurcation. As D is increased the amplitude and period of the orbit generally decrease which agrees with experimental data [4,3].

The behavior near the leftmost Hopf bifurcation is actually quite complex, as indicated in Fig. 6, which is a magnification of Fig. 3. Here the Hopf bifurcation is supercritical giving rise to a stable orbit which then undergoes a period-doubling cascade to chaos over an extremely small interval. The first period-doubling occurs at $D \approx 0.092697$ and the solution appears chaotic by $D = 0.092700$. At $D \approx 0.092701$ the attractor suddenly explodes in size and the oscillation amplitude grows considerably. As D decreases toward this point we observe a period-adding sequence. Period-adding sequences are characterized by successive jumps in the period in a manner that forms an approximately arithmetic sequence. Such sequences have been observed in models of many physical systems [21,30–32]. To our knowledge period-adding sequences are not completely understood, but seem to arise when periodic solutions interact with an invariant manifold of a saddle-type equilibrium giving rise to a Poincaré map that is piecewise-smooth and often discontinuous. Period-adding in one-dimensional piecewise-smooth maps has been the subject of recent research [20,33–35]. Dynamical behavior between period-adding windows (intervals of the bifurcation parameter within which the period undergoes no sudden change) is determined by the types and order of various

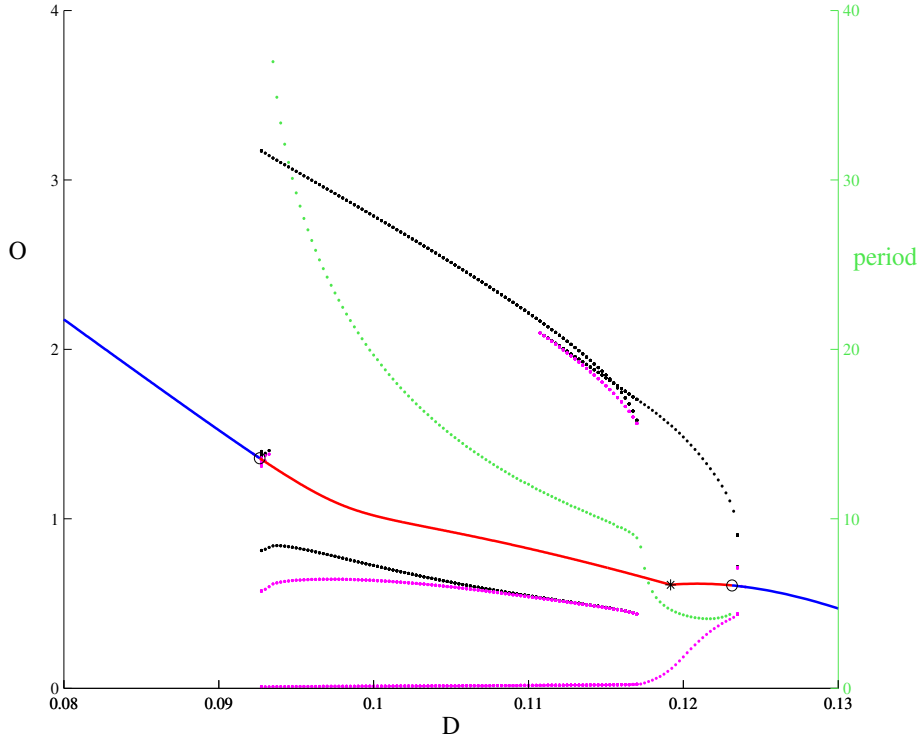

Fig. 3. A bifurcation diagram of the system (2.1) when $k_La = 150$. The equilibrium is colored blue when stable and red otherwise. Black [magenta] dots correspond to local maxima [minima] O that stable oscillations obtain. Two Hopf bifurcations are indicated by circles. The asterisk corresponds to where $r_1 < r_2 = r_3$ at equilibrium. The period of these oscillations is also indicated. (For interpretation of the references to color in this figure legend, the reader is referred to the web version of this article.)

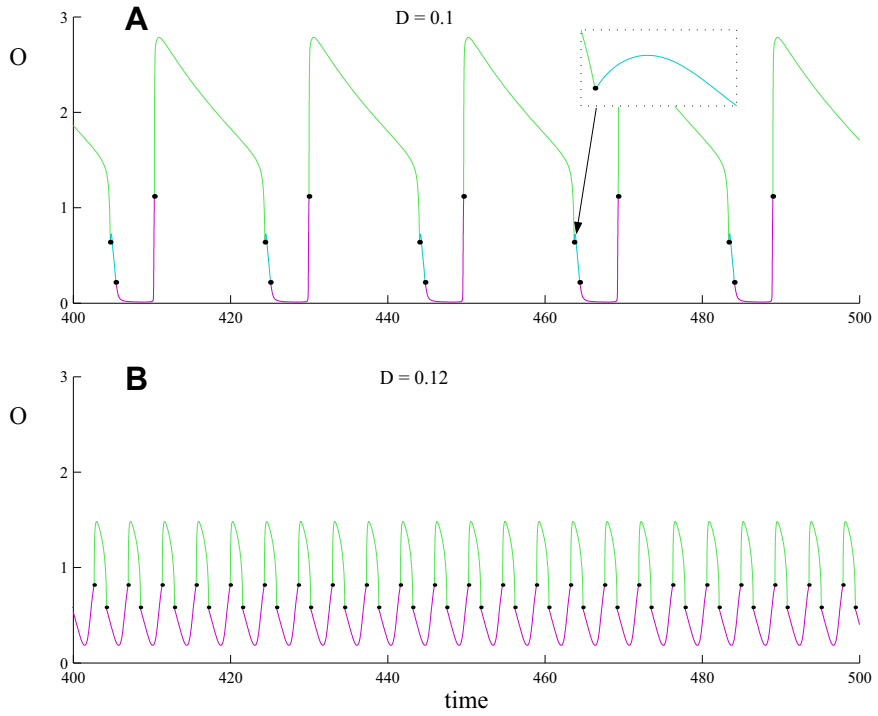

Fig. 4. Time series after transients have decayed when $k_L a = 150$, $D = 0.1$ in panel A and $D = 0.12$ in panel B. The solution is colored cyan when $r_1 = r_{max}$, magenta when $r_2 = r_{max}$ and green when $r_3 = r_{max}$. (For interpretation of the references to color in this figure legend, the reader is referred to the web version of this article.)

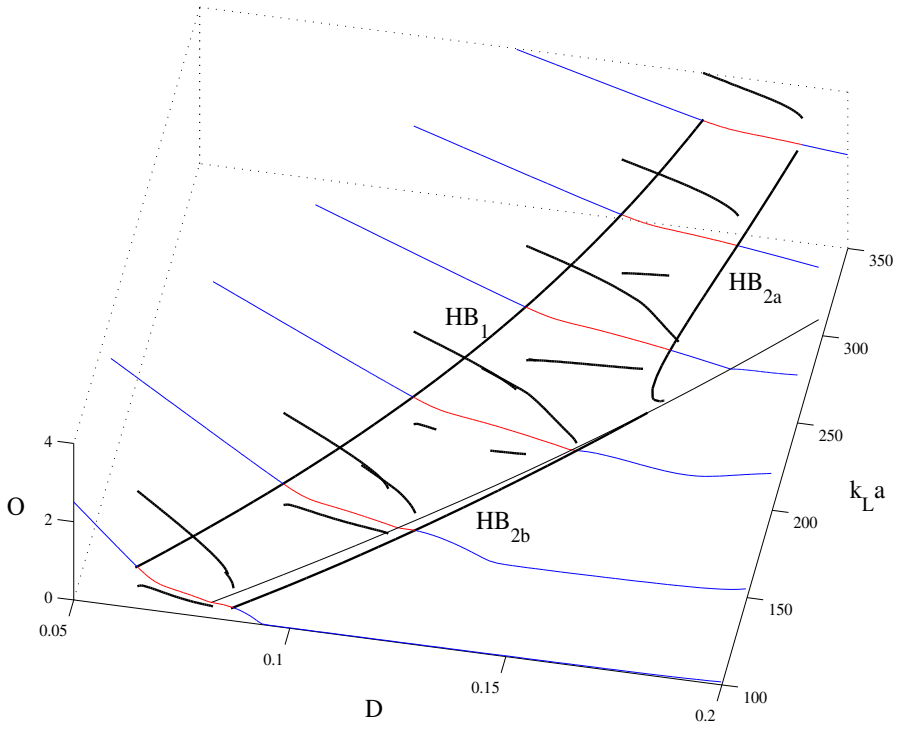

Fig. 5. Bifurcation diagrams of (2.1) at six different values of $k_L a$ with the same color scheme as Fig. 3. A curve of discontinuity and Hopf loci shown in Fig. 1 are also included. (For interpretation of the references to color in this figure legend, the reader is referred to the web version of this article.)

local bifurcations. In Fig. 6, the period appears to go to infinity in the period-adding sequence. Within the extremely small regions between windows, we have identified period-doubling bifurcations and complicated attractors although these attractors deviate only slightly from the observed periodic orbits.

5. Codimension-two discontinuous bifurcations

This section studies dynamics near two of the codimension-two, discontinuous bifurcation scenarios that were identified in Section 3. Adopting a general viewpoint, we will first unfold the

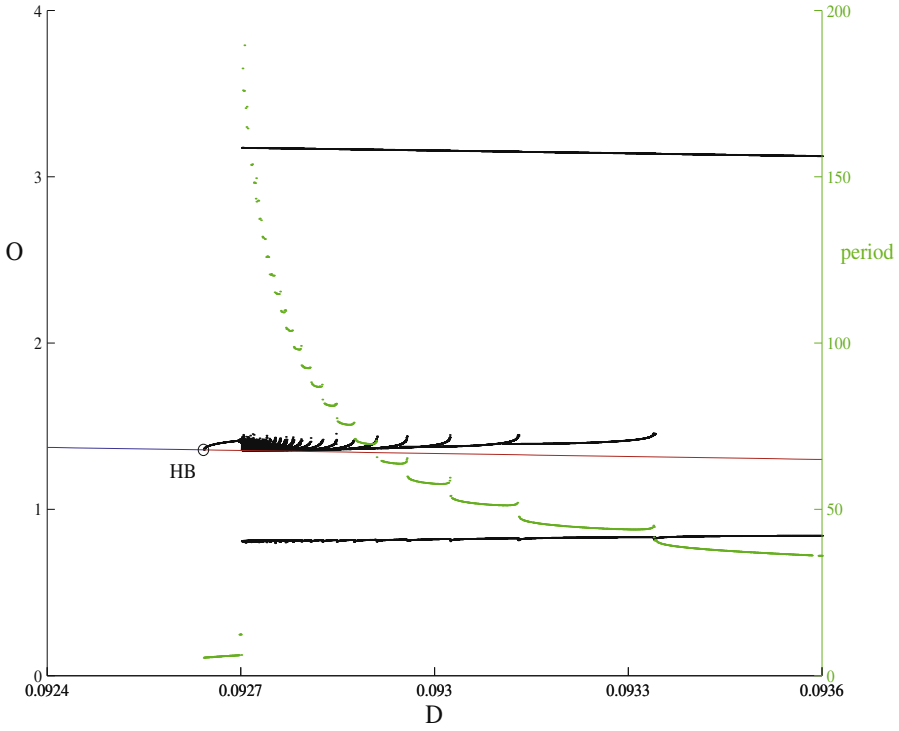

Fig. 6. A magnification of Fig. 3, near the leftmost Hopf bifurcation. Local minimums are not shown.

simultaneous occurrence of a saddle-node bifurcation and a discontinuous bifurcation; our results are summarized in Fig. 7A. The tangency illustrated in this figure matches our numerically computed bifurcation set, specifically point (e) of Fig. 2B. Secondly we will unfold the simultaneous occurrence of a Hopf bifurcation and a discontinuous bifurcation, see Fig. 7B. This theoretical prediction also matches numerical results, specifically the points (a), (c) and (d) of Fig. 2.

The results of this section are presented formally in Theorems 5.1 and 5.4, proofs of which are given in Appendix A. Proofs to Lemmas 5.2 and 5.3 are described in [27]. Throughout this section we use arbitrary parameters μ and η that do not relate to particular parameters of (2.1). To clarify our notation, $O(i)$ [$o(i)$] denotes terms that are order i or greater [greater than order i] in *every* variable and parameter on which the given expression depends.

In the neighborhood of a single switching manifold an N-dimensional, piecewise-smooth, continuous system may be written as

$$\dot{x} = \begin{cases} f^{(L)}(x;\mu,\eta), & H(x;\mu,\eta) \leqslant 0 \\ f^{(R)}(x;\mu,\eta), & H(x;\mu,\eta) \geqslant 0 \end{cases}, \tag{5.1}$$

where $f^{(L)}, f^{(R)} : \mathbb{R}^N \times \mathbb{R}^2 \to \mathbb{R}^N$ are C^k and we assume that $H : \mathbb{R}^N \times \mathbb{R}^2 \to \mathbb{R}$ is sufficiently smooth (at least C^4). The switching manifold is the parameter dependent set, $\mathscr{S}_{\mu,\eta} = \{x \in \mathbb{R}^N : H(x;\mu,\eta) = 0\}$. If, when $(x;\mu,\eta) = (0;0,0)$, we have $H = 0$ and $\nabla_x H \neq 0$ then locally $\mathscr{S}_{0,0}$ is a $(N-1)$-dimensional manifold intersecting the origin. Via coordinate transformations in a similar manner to those given in [26], we may assume, to order C^4, that H is simply equal to x_1. The higher order terms in H do not affect our analysis below; thus for simplicity, in what follows we will assume H is identically equal to x_1. The switching manifold is then the plane $x_1 = 0$ and we will refer to $f^{(L)}$ as the *left-half-system* and $f^{(R)}$ as the *right-half-system*.

We assume that when $\mu = \eta = 0$, the origin is an equilibrium. Since the origin lies on the switching manifold and (5.1) is continuous, it is an equilibrium of both left- and right-half-systems. We will assume

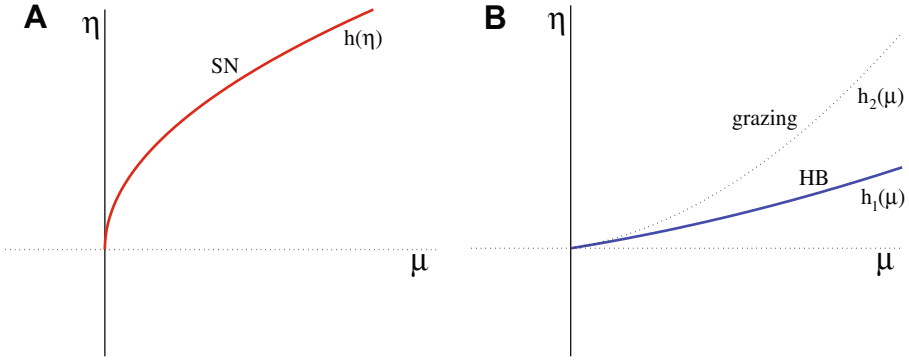

Fig. 7. Unfoldings predicted by Theorems 5.1 and 5.4. SN, saddle-node bifurcation; HB, Hopf bifurcation. Along the curve labeled 'grazing', the Hopf cycle intersects the switching manifold at one point. Along the η-axis, an equilibrium lies on the switching manifold.

$$\det(D_x f^{(R)}(0;0,0)) \neq 0; \tag{5.2}$$

that is, for the right-half-system, zero is not an associated eigenvalue of the origin when $\mu = \eta = 0$. Then by the implicit function theorem the right-half-system has an equilibrium, $x^{*(R)}(\mu,\eta)$, with $x^{*(R)}(0,0) = 0$ and that depends upon the parameters as a C^k function in some neighborhood of the origin. As is generically the case, we may assume the distance the equilibrium is from the switching manifold varies linearly with some linear combination of the parameters. Without loss of generality we may assume μ is a suitable choice; that is

$$\frac{\partial x_1^{*(R)}(0,0)}{\partial \mu} \neq 0. \tag{5.3}$$

In this case, the implicit function theorem implies there is a C^k function $\phi_1 : \mathbb{R} \to \mathbb{R}$ such that $x_1^{*(R)}(\phi_1(\eta),\eta) = 0$. In other words when $\mu = \phi(\eta)$, the equilibrium lies on the switching manifold. By performing the nonlinear change of coordinates

$$\mu \mapsto \mu - \phi_1(\eta),$$
$$x \mapsto x - x^{*(R)}(\phi_1(\eta),\eta),$$

we may factor μ out of the constant term in the system, i.e.,

$$f^{(L)}(0;\mu,\eta) = f^{(R)}(0;\mu,\eta) = \mu b(\mu,\eta) + o(k),$$

where b is C^{k-1}. Notice the transformation does not alter the switching manifold. The system is now

$$\dot{x} = \begin{cases} f^{(L)}(x;\mu,\eta), & x_1 \leqslant 0 \\ f^{(R)}(x;\mu,\eta), & x_1 \geqslant 0 \end{cases}, \tag{5.4}$$

with

$$f^{(i)}(x;\mu,\eta) = \mu b(\mu,\eta) + A_i(\mu,\eta)x + O(|x|^2) + o(k), \tag{5.5}$$

where A_L and A_R are $N \times N$ matrices that are C^{k-1} functions of μ and η.

Since (5.4) is continuous, the matrices A_L and A_R have matching elements in all but possibly their first columns. It directly follows that the *adjugate* matrices (if A is non-singular, then $\mathrm{adj}(A) \equiv \det(A)A^{-1}$) of A_L and A_R share the same first row

$$\xi^{\mathsf{T}} = e_1^{\mathsf{T}}\mathrm{adj}(A_L) = e_1^{\mathsf{T}}\mathrm{adj}(A_R). \tag{5.6}$$

To understand the role of the vector, ξ, consider equilibria of (5.4). When $\mu = \eta = 0$, the origin is an equilibrium. For small non-zero μ each half-system has an equilibrium, $x^{*(i)}$, with first component

$$x_1^{*(i)}(\mu,\eta) = -\left.\frac{\xi^{\mathsf{T}}b}{\det(A_i)}\right|_{\mu=\eta=0}\mu + O(2),$$

provided that $\det(A_i(0,0)) \neq 0$. Notice that our non-degeneracy assumption (5.3), is satisfied if $\xi^{\mathsf{T}}(0,0)b(0,0) \neq 0$. If $x_1^{*(R)} \geqslant 0$, then $x^{*(R)}$ is an equilibrium of the piecewise-smooth system (5.4) and is said to be *admissible*, otherwise it is *virtual*. Similarly $x^{*(L)}$ is admissible if and only if $x_1^{*(L)} \leqslant 0$. Finally, notice if $\det(A_L(0,0))$ and $\det(A_R(0,0))$ are of the same sign, then $x^{*(L)}$ and $x^{*(R)}$ are admissible for different signs of μ, whereas if $\det(A_L(0,0))$ and $\det(A_R(0,0))$ have opposite sign, $x^{*(L)}$ and $x^{*(R)}$ are admissible for the same sign of μ. The former case is known as *persistence*; the latter is known as a *non-smooth fold* [20].

The following theorem describes dynamical phenomena near $\mu = \eta = 0$ when $\det(A_L(0,0)) = 0$.

Theorem 5.1. *Consider the system (5.4) with (5.5) and assume that $k \geqslant 4$. Suppose that near $(\mu,\eta) = (0,0)$, $A_L(\mu,\eta)$ has an eigenvalue $\lambda(\mu,\eta) \in \mathbb{R}$ with the associated eigenvector, $v(\mu,\eta)$. In addition, suppose*

(i) $\lambda(0,0) = 0$ is of algebraic multiplicity 1 and is the only eigenvalue of $A_L(0,0)$ with zero real part,

(ii) $\xi(0,0)^{\mathsf{T}}b(0,0) \neq 0$.

Then $v(0,0)$ has a non-zero first component and the magnitude of $v(0,0)$ may be scaled such that, $\xi(0,0)^{\mathsf{T}}v(0,0) = 1$. Finally suppose that

(iii) $\frac{\partial\lambda}{\partial\eta}(0,0) \neq 0$,

(iv) $a_0 = \xi^{\mathsf{T}}((D_x^2 f^{(L)})(v,v))|_{(0,0,0)} \neq 0$.

Then there exists a unique C^{k-2} function $h : \mathbb{R} \to \mathbb{R}$ with $h(0) = h'(0) = 0$ and

$$h''(0) = \left.\frac{\left(\frac{\partial\lambda}{\partial\eta}\right)^2}{a_0\xi^{\mathsf{T}}b}\right|_{(0,0)}, \tag{5.7}$$

such that in a neighborhood of $(\mu,\eta) = (0,0)$, the curve $\mu = h(\eta)$ corresponds to a locus of saddle-node bifurcations of equilibria of (5.4) that are admissible when

$$\mathrm{sgn}(\eta) = \mathrm{sgn}\left(a_0 v_1 \frac{\partial\lambda}{\partial\eta}\right)\Big|_{(0,0)}. \tag{5.8}$$

A proof of Theorem 5.1 is given in Appendix A. The theorem implies a bifurcation diagram like that depicted in Fig. 7A. In particular the curve of saddle-node bifurcations is tangent to the η-axis as shown.

The second theorem, Theorem 5.4, describes dynamical phenomena near $\mu = \eta = 0$ when $A_L(0,0)$ has a purely imaginary complex eigenvalue pair. The method of proof is essentially a standard dimension reduction by restriction to the center manifold of the left-half-system The dynamics of the resulting planar system are determined by the following two lemmas. Lemma 5.3 provides a transformation of the planar system to observer canonical form [20]. Lemma 5.2 describes local dynamics of the planar system in this canonical form.

Lemma 5.2. *Consider the two-dimensional C^k ($k \geqslant 5$) system*

$$\begin{bmatrix}\dot{x}\\ \dot{y}\end{bmatrix} = \begin{bmatrix} f(x,y;\mu,\eta)\\ g(x,y;\mu,\eta)\end{bmatrix} = \begin{bmatrix}0\\ -\mu\end{bmatrix} + \begin{bmatrix}\eta & 1\\ -\delta(\mu,\eta) & 0\end{bmatrix}\begin{bmatrix}x\\ y\end{bmatrix} + O(|x,y|^2) + o(k). \tag{5.9}$$

Suppose,

(i) $\delta(0,0) = \omega^2$ for $\omega > 0$,

(ii) $a_0 \neq 0$, where

$$a_0 = \frac{1}{16}(f_{xxx} + g_{xxy} + \omega^2 f_{xyy} + \omega^2 g_{yyy}) - \frac{1}{16}f_{xy}(f_{xx} + \omega^2 f_{yy}) + \frac{1}{16}g_{xy}\left(\frac{1}{\omega^2}g_{xx} + g_{yy}\right) + \frac{1}{16}\left(\frac{1}{\omega^2}f_{xx}g_{xx} - \omega^2 f_{yy}g_{yy}\right) \tag{5.10}$$

evaluated at $(x,y;\mu,\eta) = (0,0;0,0)$. Then, near $(x,y;\mu,\eta) = (0,0;0,0)$, there is a unique equilibrium given by C^k functions

$$x^*(\mu,\eta) = -\frac{1}{\omega^2}\mu + O(2),$$
$$y^*(\mu,\eta) = O(2),$$

and there exist C^{k-1}, C^{k-2} functions $h_1, h_2 : \mathbb{R} \to \mathbb{R}$ respectively, with

$$h_1(\mu) = \left.\frac{1}{\omega^2}(f_{xx} + g_{xy})\right|_{(0,0;0,0)}\mu + O(\mu^2), \tag{5.11}$$

$$h_2(\mu) = h_1(\mu) - \frac{2a_0}{\omega^4}\mu^2 + O(\mu^3), \tag{5.12}$$

such that for small μ, the curve $\eta = h_1(\mu)$ corresponds to Andronov–Hopf bifurcations of $(x^*,y^*)^{\mathsf{T}}$ and the curve $\eta = h_2(\mu)$ corresponds to associated Hopf cycles intersecting the y-axis tangentially at one point. The Hopf bifurcations are supercritical if $a_0 < 0$ and subcritical if $a_0 > 0$. The Hopf cycle lies entirely in the left-half-plane if and only if $\mu > 0$ and η lies between $h_1(\mu)$ and $h_2(\mu)$.

Lemma 5.3. *Consider the system (5.4) with (5.5) and assume that $N = 2$ and $k \geqslant 5$. Suppose $A_L(\mu,\eta)$ has complex eigenvalues $\lambda_\pm = \nu \pm i\omega$ with*

(i) $\nu(0,0) = 0$ and $\omega(0,0) > 0$,
(ii) $\frac{\partial \nu}{\partial \eta}(0,0) \neq 0$,
(iii) $\xi^T(0,0)b(0,0) \neq 0$.

Then there is a nonlinear transformation not altering the switching manifold such that the left-half-flow of (5.4) is given by (5.9). All conditions in Lemma 5.2 will be satisfied except possibly the non-degeneracy condition, $a_0 \neq 0$.

Theorem 5.4. *Consider the system (5.4) with (5.5) and assume that $N > 2$ and $k \geqslant 6$. Suppose near $(\mu,\eta) = (0,0)$, $A_L(\mu,\eta)$ has complex eigenvalues $\lambda_\pm = \nu \pm i\omega$ with associated eigenvectors, $z_\pm = u^{(1)} \pm iu^{(2)}$. Suppose*

(i) $\nu(0,0) = 0$, $\omega(0,0) > 0$, and $A_L(0,0)$ has no other eigenvalues on the imaginary axis,
(ii) $\frac{\partial \nu}{\partial \eta}(0,0) \neq 0$,
(iii) $\xi^T(0,0)b(0,0) \neq 0$,
(iv) either $u_1^{(1)}$ or $u_1^{(2)}$ is non-zero.

Then, in the extended coordinate system (x,μ,η), there exists a C^{k-1} four-dimensional center manifold, W^c, for the left-half-system that passes through the origin and is not tangent to the switching manifold at this point. Furthermore, $\exists i \neq 1$, such that in the coordinate system

$$\begin{bmatrix} \hat{x}_1 \\ \hat{x}_2 \end{bmatrix} = \begin{bmatrix} x_1 \\ x_i \end{bmatrix},$$

the left-half-flow of (5.4) restricted to W^c is given by (5.4) with $N = 2$ (with 'hatted' variables) and all conditions in Lemma 5.3 will be satisfied.

See Appendix A for a proof. Theorem 5.4 implies that an N-dimensional system near a codimension-two point with a simultaneous Hopf and discontinuous bifurcation will have a bifurcation diagram like that shown in Fig. 7B. In particular, the curves of grazing and Hopf bifurcations are tangent to one another at the origin. For this scenario in two dimensions it is known that a curve of saddle-node bifurcations of the Hopf cycle may exist very close to the grazing curve [27]. We have not been able to extend this result to higher dimensions.

6. Conclusions

In this paper we investigated the onset of stable oscillations and more complex behavior in a model of *S. cerevisiae* growth taken from [9]. The model assumes an instantaneous switching between competing metabolic pathways resulting in a piecewise-smooth, continuous system of ODEs. In this paper we identified a variety of discontinuity induced bifurcations.

The model exhibits stable oscillations that arise from Andronov–Hopf bifurcations for intermediate values of the dilution rate, D; these have also been observed experimentally. As D grows, the oscillation amplitude suddenly jumps to a much larger value just slightly beyond the Hopf bifurcation. We do not have a detailed explanation for this sudden amplitude change. As D is increased further, the resulting stable orbits undergo a complex sequence of bifurcations causing their periods and amplitudes to decrease, until a second Hopf bifurcation occurs resulting again in a stable equilibrium.

For the model (2.1), a change in the preferred metabolic pathway at an equilibrium results in the loss of differentiability for orbits in its neighborhood. The result is often a discontinuous bifurcation and we have identified discontinuous saddle-node and Hopf bifurcations. The system also exhibits codimension-two bifurcations that correspond to simultaneous discontinuous and saddle-node or Hopf bifurcations. We have provided a rigorous unfolding of these scenarios from a general viewpoint.

While the behavior that we studied are specific to piecewise-smooth, continuous models, a model in which this simplification is relaxed should still have much the same behavior. For example if the relative strength of two competing pathways reverses, then exponential growth will lead to the dominance of one over the other over a small parameter range and a short timescale. Though the bifurcations generic to smooth systems are restricted relative to those of discontinuous systems, a rapid sequence of these bifurcations over a small range of parameters may lead to the same behavior on a rougher scale as the discontinuous one. This can be seen, for example, in the simplest models such as a smoothed one-dimensional tent map.

Appendix A. Proofs

Proof of Theorem 5.1

Recall, for any $N \times N$ matrix, A,

$$\mathrm{adj}(A)A = \det(A)I.$$

By putting $A = A_L(0,0)$, multiplying on the left by e_1^T and using (5.6) we obtain

$$\xi^T(0,0)A_L(0,0) = 0.$$

Thus $\xi^T(0,0)$ is the left eigenvector of $A_L(0,0)$ for $\lambda(0,0) = 0$. Consequently we may indeed choose the length of the right eigenvector $v(0,0)$ such that $\xi^T(0,0)v(0,0) = 1$.

Now we show $v(0,0)$ has a non-zero first element. Suppose for a contradiction, $v_1(0,0) = 0$. Let B_{ij} denote the $(N-1)\times(N-1)$ matrix formed by removing the ith row and jth column from $A_L(0,0)$. Let $\tilde{v} = (v_2(0,0),\ldots,v_N(0,0))^T \in \mathbb{R}^{N-1}$. Then $\tilde{v} \neq 0$ and $B_{i1}\tilde{v} = 0$ for each i. Therefore each $\det(B_{i1}) = 0$, i.e., each element in the first column of the cofactor matrix of $A_L(0,0)$ is zero. Thus $\xi^T(0,0) = 0$ which is a contradiction. Therefore

$$v_1(0,0) \neq 0.$$

Let $v^{(1)},\ldots,v^{(N)}$ be N generalized eigenvectors of $A_L(0,0)$ that form a basis of $\mathbb{R}^N$ with $v^{(1)} = v(0,0)$. Let $V = [v^{(1)}\cdots v^{(N)}]$. We introduce the linear change of coordinates

$$\hat{x} = V^{-1}x. \tag{A.1}$$

Let

$$F = \begin{bmatrix} \dot{\hat{x}} \\ \dot{\mu} \\ \dot{\eta} \end{bmatrix} = \begin{bmatrix} V^{-1}f^{(L)}(V\hat{x};\mu,\eta) \\ 0 \\ 0 \end{bmatrix}, \tag{A.2}$$

denote the $(N+2)$-dimensional C^k extended left-half-flow in the basis of generalized eigenvectors. The Jacobian

$$DF(0;0,0) = \left[\begin{array}{c|c|c} V^{-1}A_L(0,0)V & V^{-1}b(0,0) & 0 \\ \hline 0 & 0 & 0 \end{array}\right], \tag{A.3}$$

has a three-dimensional nullspace, E^c. The $(N+2)$-dimensional vectors

$$\{n_1, n_2, n_3\} = \left\{ e_1, \begin{bmatrix} \varphi \\ 1 \\ 0 \end{bmatrix}, e_{N+2} \right\},$$

where n_2 is a generalized eigenvector and $\varphi \in \mathbb{R}^N$, span E^c. The local center manifold, W^c, is tangent to E^c, thus on W^c,

$$\hat{x} = H(\hat{x}_1; \mu, \eta) = \hat{x}_1 e_1 + \mu\zeta + O(2),$$

where $\zeta \in \mathbb{R}^N$ is equal to φ except that its first element is zero. Notice $\xi^{\mathsf{T}}(0,0)V = e_1^{\mathsf{T}}$ thus

$$\hat{x}_1 = e_1^{\mathsf{T}}\hat{x} = \xi^{\mathsf{T}}(0,0)V\hat{x} = \xi^{\mathsf{T}}(0,0)x.$$

Restricted to W^c the dynamics (A.2) become the C^{k-1} system

$$\begin{aligned}\dot{\hat{x}}_1 = {} & \mu\xi^{\mathsf{T}}(0,0)b(\mu,\eta) + \xi^{\mathsf{T}}(0,0)A_L(\mu,\eta)VH(\hat{x}_1;\mu,\eta) \\ & + \xi^{\mathsf{T}}(0,0)g^L(VH(\hat{x}_1;\mu,\eta);\mu,\eta),\end{aligned} \tag{A.4}$$

where $g^L(x;\mu,\eta)$ denotes all terms of f^L that are nonlinear in x. By expanding each term in (A.4) to second order we obtain

$$\begin{aligned}\dot{\hat{x}}_1(\hat{x}_1;\mu,\eta) = {} & c_1\mu + c_2\hat{x}_1^2 + c_3\hat{x}_1\eta + c_4\hat{x}_1\mu + c_5\mu^2 + c_6\mu\eta \\ & + O(3),\end{aligned} \tag{A.5}$$

where, in particular

$$\begin{aligned} c_1 &= \xi(0,0)^{\mathsf{T}} b(0,0), \\ c_2 &= \frac{a_0}{2}, \\ c_3 &= \frac{\partial\lambda}{\partial\eta}(0,0). \end{aligned}$$

Let $\hat{x}_1^*$ be an equilibrium of (A.5). Since $c_1 \neq 0$ by hypothesis, by the implicit function theorem there exists a unique C^{k-1} function, $\mu_{\text{eq}}(\hat{x}_1^*, \eta)$ such that $\dot{\hat{x}}_1(\hat{x}_1^*; \mu_{\text{eq}}(\hat{x}_1^*,\eta),\eta) = 0$ and

$$\mu_{\text{eq}}(\hat{x}_1^*,\eta) = -\frac{c_2}{c_1}\hat{x}_1^{*2} - \frac{c_3}{c_1}\hat{x}_1^*\eta + O(3).$$

Near $(\mu,\eta) = (0,0)$, the linearization about the equilibrium $\hat{x}_1^*$, has an associated eigenvalue of 0 exactly when

$$0 = \frac{\partial\dot{\hat{x}}_1}{\partial\hat{x}_1}(\hat{x}_1^*; \mu_{\text{eq}}(\hat{x}_1^*,\eta),\eta) = 2c_2\hat{x}_1^* + c_3\eta + O(2). \tag{A.6}$$

Since $a_0 \neq 0$ by hypothesis, the implicit function theorem again implies there exists a unique C^{k-2} function, $\hat{h} : \mathbb{R} \to \mathbb{R}$ such that, (A.6) is satisfied when $\hat{x}_1^* = \hat{h}(\eta)$ and

$$\hat{h}(\eta) = -\frac{c_3}{2c_2}\eta + O(\eta^2). \tag{A.7}$$

The function

$$h(\eta) = \mu_{\text{eq}}(\hat{h}(\eta),\eta) = \frac{c_3^2}{4c_1c_2}\eta^2 + O(\eta^3), \tag{A.8}$$

is C^{k-2}. We now show saddle-node bifurcations occur for the left-half-flow on the curve $\mu = h(\eta)$ when η is small by verifying the three conditions of the saddle-node bifurcation theorem, see for instance [36]:

(i) by construction, $D_x f^L(x^*; h(\eta),\eta)$ has a zero eigenvalue of algebraic multiplicity 1, and there are no other eigenvalues with zero real part when η is sufficiently small,
(ii) $w(\mu,\eta)\frac{\partial f^L}{\partial\mu}(x^*; h(\eta),\eta) = \xi^{\mathsf{T}}(0,0)b(0,0) + O(\eta) \neq 0$ where $w(\mu,\eta)$ is the left eigenvector of $A_L(\mu,\eta)$ for $\lambda(\mu,\eta)$,
(iii) $w(\mu,\eta)(D_x^2 f^L(x^*; h(\eta),\eta)(v(\mu,\eta), v(\mu,\eta))) = a_0 + O(\eta) \neq 0$.

Finally, notice that on W^c

$$x_1 = e_1^{\mathsf{T}}VH(\hat{x}_1;\mu,\eta) = v_1(0,0)\hat{x}_1 + O(2) \neq 0,$$

and by (A.7), when $\mu = h(\eta)$

$$x_1^* = -\frac{c_3 v_1(0,0)}{2c_2}\eta + O(\eta^2).$$

Thus the equilibrium at the saddle-node bifurcation is admissible when $\text{sgn}(\eta) = \text{sgn}(c_2c_3v_1(0,0)) = \text{sgn}(a_0 v_1 \frac{\partial\lambda}{\partial\eta})\big|_{(0,0)}$. □

Proof of Theorem 5.4

Since the real and imaginary parts of the eigenvectors $z_\pm$, $u^{(1)}$ and $u^{(2)}$, are linearly independent, there exists an $i \neq 1$ such that

$$U = \begin{bmatrix} u_1^{(1)} & u_1^{(2)} \\ u_i^{(1)} & u_i^{(2)} \end{bmatrix},$$

is non-singular. For the remainder of this proof we will set $i = 2$, w.l.o.g. Define two new vectors by

$$[v^{(1)}\, v^{(2)}] = [u^{(1)} u^{(2)}]U^{-1}, \tag{A.9}$$

let

$$V = [v^{(1)}\, v^{(2)} e_3 \cdots e_N],$$

and introduce the new coordinate system

$$\hat{x} = V^{-1}x. \tag{A.10}$$

Note the inclusion of the matrix, U^{-1}, in (A.9) allows for simplification below, in particular, $e_i^{\mathsf{T}}V = e_i^{\mathsf{T}}V^{-1} = e_i^{\mathsf{T}}$ for $i = 1, 2$. The $(N+2)$-dimensional C^k extended left-half-flow in the new coordinates is given by (A.2) as before. The Jacobian, $DF(0;0,0)$, (A.3), has a four-dimensional linear center manifold, E^c, spanned by

$$\{n_1, n_2, n_3, n_4\} = \left\{ e_1, e_2, \begin{bmatrix} -(A_L(0,0)V)^{-1}b \\ 1 \\ 0 \end{bmatrix}, e_{N+2} \right\}.$$

Notice W^c is not tangent to the switching manifold by condition (iv) of the theorem. On the local center manifold

$$\hat{x} = H(\hat{x}_1, \hat{x}_2; \mu, \eta) = \hat{x}_1 e_1 + \hat{x}_2 e_2 + \zeta\mu + O(2),$$

where $\zeta \in \mathbb{R}^N$ is equal to $-(A_L(0,0)V)^{-1}b$ except that its first two elements are zero. The dynamics on W^c are described by

$$\begin{aligned}\begin{bmatrix} \dot{\hat{x}}_1 \\ \dot{\hat{x}}_2 \end{bmatrix} = {} & \begin{bmatrix} e_1^{\mathsf{T}} \\ e_2^{\mathsf{T}} \end{bmatrix}(V^{-1}\mu b + V^{-1}A_L VH(\hat{x}_1,\hat{x}_2;\mu,\eta) \\ & + V^{-1}g^{(L)}(VH(\hat{x}_1,\hat{x}_2;\mu,\eta);\mu,\eta)),\end{aligned}$$

where $g^{(L)}$ represents all terms of $f^{(L)}$ that are nonlinear in x. By using (A.9) and

$$A_L[u^{(1)}u^{(2)}] = [u^{(1)}u^{(2)}]D,$$

where, at $\mu = \eta = 0$,

$$D = \begin{bmatrix} v & \omega \\ -\omega & v \end{bmatrix},$$

we obtain

$$\begin{bmatrix} \dot{\hat{x}}_1 \\ \dot{\hat{x}}_2 \end{bmatrix} = \mu\hat{b}(\mu,\eta) + \widehat{A}_L(\mu,\eta)\begin{bmatrix} \hat{x}_1 \\ \hat{x}_2 \end{bmatrix} + O(2), \tag{A.11}$$

where

$$\widehat{A}_L = \begin{bmatrix} e_1^{\mathsf{T}} \\ e_2^{\mathsf{T}} \end{bmatrix} V^{-1}A_L V[e_1 e_2] = UDU^{-1},$$

and

$$\begin{aligned}\hat{b} &= \begin{bmatrix} e_1^{\mathsf{T}} \\ e_2^{\mathsf{T}} \end{bmatrix} V^{-1}b - \begin{bmatrix} e_1^{\mathsf{T}} \\ e_2^{\mathsf{T}} \end{bmatrix} V^{-1}A_L V\zeta = \begin{bmatrix} e_1^{\mathsf{T}} \\ e_2^{\mathsf{T}} \end{bmatrix} V^{-1}A_L[v^{(1)}\, v^{(2)} 0 \cdots 0]A_L^{-1}b \\ &= [\widehat{A}_L 0 \cdots 0]A_L^{-1}b.\end{aligned}$$

Table B1
Parameter values used for all numerical investigations in this paper.

G_0	$10\ \mathrm{g\,L^{-1}}$
Y_1	$0.16\ \mathrm{g\,g^{-1}}$
Y_2	$0.75\ \mathrm{g\,g^{-1}}$
Y_3	$0.60\ \mathrm{g\,g^{-1}}$
ϕ_1	0.403
ϕ_2	$2000\ \mathrm{mg\,g^{-1}}$
ϕ_3	$1000\ \mathrm{mg\,g^{-1}}$
ϕ_4	0.95
O^*	$7.5\ \mathrm{mg\,L^{-1}}$
α	$0.3\ \mathrm{g\,g^{-1}\,h^{-1}}$
α^*	$0.1\ \mathrm{g\,g^{-1}\,h^{-1}}$
β	$0.7\ \mathrm{h^{-1}}$
K_1	$0.05\ \mathrm{g\,L^{-1}}$
K_2	$0.01\ \mathrm{g\,L^{-1}}$
K_3	$0.001\ \mathrm{g\,L^{-1}}$
K_{O_2}	$0.01\ \mathrm{mg\,L^{-1}}$
K_{O_3}	$2.2\ \mathrm{mg\,L^{-1}}$
γ_1	10
γ_2	10
γ_3	$0.8\ \mathrm{g\,g^{-1}}$
$\mu_{1,\max}$	$0.44\ \mathrm{h^{-1}}$
$\mu_{2,\max}$	$0.19\ \mathrm{h^{-1}}$
$\mu_{3,\max}$	$0.36\ \mathrm{h^{-1}}$

Finally, it is easily verified that

$$\hat{\xi}^{\mathsf{T}}\hat{b} = \frac{\det(\widehat{A}_L)}{\det(A_L)}\xi^{\mathsf{T}}b \neq 0,$$

where $\hat{\xi}^{\mathsf{T}} = e_1^{\mathsf{T}}\mathrm{adj}(\widehat{A}_L)$. □

Appendix B. Functions and parameter values

The following is a complete list of functions that are present in the model

$$\mu_i = \mu_{i,\max}\frac{\mu_{i,\max}+\beta}{\alpha+\alpha^*}, \quad i=1,2,3,$$

$$r_1 = \mu_1 e_1 \frac{G}{K_1+G},$$

$$r_2 = \mu_2 e_2 \frac{E}{K_2+E}\frac{O}{K_{O_2}+O},$$

$$r_3 = \mu_3 e_3 \frac{G}{K_3+G}\frac{O}{K_{O_3}+O},$$

$$u_i = \frac{r_i}{\sum_j r_j}, \quad i=1,2,3,$$

$$v_i = \frac{r_i}{\max_j r_j}, \quad i=1,2,3.$$

References

[1] J.E. Bailey, D.E. Ollis, Biochemical Engineering Fundamentals, McGraw-Hill, New York, 1986.
[2] H.K. Fiechter, A. von Meyenburg. Regulatory properties of growing cell populations of *Saccharomyces cerevisiae* in a continuous culture system, in: A. Kocková-Kratochrílová (Ed.), Yeasts, Proceedings of the Second Symposium on Yeasts Held in Bratislava, 16–21 July 1966, Slovenskej Akadémie Vied, Bratislava, 1968, pp. 387–398.
[3] H.K. von Meyenburg, Stable synchrony oscillations in continuous cultures of *Saccharomyces cerevisiae* under glucose limitation, in: B. Chance, E.K. Pye, T.K. Ghosh, B. Hess (Eds.), Biological and Biochemical Oscillators, Academic Press, New York, 1973, p. 411.
[4] D. Porro, E. Martegani, B.M. Ranzi, L. Alberghina, Oscillations in continuous cultures of budding yeast: a segregated parameter analysis, Biotechnol. Bioeng. 32 (1988) 411.
[5] A.D. Satroutdinov, H. Kuriyama, H. Kobayashi, Oscillatory metabolism of *Saccharomyces cerevisiae* in continuous culture, FEMS Microbiol. Lett. 98 (1992) 261.
[6] P. Richard, The rhythm of yeast, FEMS Microbiol. Rev. 27 (2003) 547.
[7] M.A. Henson, Dynamic modeling and control of yeast cell populations in continuous biochemical reactors, Comput. Chem. Eng. 27 (2003) 1185.
[8] S. Danø, F. Hynne, S. De Monte, F. d'Ovidio, P.G. Sørensen, H. Westerhoff, Synchronization of glycolytic oscillations in a yeast cell population, Faraday Discuss. 120 (2001) 261.
[9] K.D. Jones, D.S. Kompala, Cybernetic model of the growth dynamics of *Saccharomyces cerevisiae* in batch and continuous cultures, J. Biotechnol. 71 (1999) 105.
[10] M. Wiercigroch, B. De Kraker (Eds.), Applied Nonlinear Dynamics and Chaos of Mechanical Systems with Discontinuities, World Scientific Press, Singapore, 2000.
[11] B. Brogliato, Nonsmooth Mechanics: Models, Dynamics and Control, Springer, New York, 1999.
[12] R.I. Leine, H. Nijmeijer, Dynamics and bifurcations of non-smooth mechanical systems, in: Lecture Notes in Applied and Computational Mathematics, vol. 18, Springer, Berlin, 2004.
[13] S. Banerjee, G.C. Verghese (Eds.), Nonlinear Phenomena in Power Electronics, IEEE Press, New York, 2001.
[14] Z.T. Zhusubaliyev, E. Mosekilde, Bifurcations and Chaos in Piecewise-Smooth Dynamical Systems, World Scientific Press, Singapore, 2003.
[15] C.K. Tse, Complex Behavior of Switching Power Converters, CRC Press, Boca Raton, FL, 2003.
[16] T. Puu, I. Sushko (Eds.), Business Cycle Dynamics: Models and Tools, Springer, New York, 2006.
[17] E. Mosekilde, J.L. Laugesen, Nonlinear dynamic phenomena in the beer model, Syst. Dyn. Rev. 23 (2007) 229.
[18] R. Rosen, Dynamical System Theory in Biology, Wiley–Interscience, New York, 1970.
[19] J. Keener, J. Sneyd, Mathematical Physiology, Springer, New York, 1998.
[20] M. di Bernardo, C.J. Budd, A.R. Champneys, P. Kowalczyk, Piecewise-smooth Dynamical Systems. Theory and Applications, Springer, New York, 2008.
[21] P.T. Piiroinen, L.N. Virgin, A.R. Champneys, Chaos and period-adding: experimental and numerical verification of the grazing bifurcation, J. Nonlinear Sci. 14 (4) (2004) 383.
[22] E. Freire, E. Ponce, F. Rodrigo, F. Torres, Bifurcation sets of continuous piecewise linear systems with two zones, Int. J. Bifurcat. Chaos 8 (11) (1998) 2073.
[23] E. Freire, E. Ponce, J. Ros, A biparametric bifurcation in 3D continuous piecewise linear systems with two zones. Application to Chua's circuit, Int. J. Bifurcat. Chaos 17 (2) (2007) 445.
[24] V. Carmona, E. Freire, E. Ponce, F. Torres, The continuous matching of two stable linear systems can be unstable, Discrete Contin. Dyn. Syst. 16 (3) (2006) 689.
[25] K.D. Jones, Cybernetic modeling of spontaneous oscillations in continuous cultures of *Saccharomyces cerevisiae*, Master's thesis, University of Colorado, Boulder, CO, 1995.
[26] M. di Bernardo, C.J. Budd, A.R. Champneys, Normal form maps for grazing bifurcations in *n*-dimensional piecewise-smooth dynamical systems, Physica D 160 (2001) 222.
[27] D.J.W. Simpson, J.D. Meiss, Unfolding a codimension-two discontinuous Andronov–Hopf bifurcation, Chaos 18 (3) (2008) 033125.
[28] Yu.A. Kuznetsov, Elements of bifurcation theory, in: Appl. Math. Sci., vol. 112, Springer, New York, 2004.
[29] S.J. Parulekar, G.B. Semones, M.J. Rolf, J.C. Lievense, H.C. Lim, Induction and elimination of oscillations in continuous cultures of *Saccharomyces cerevisiae*, Biotechnol. Bioeng. 28 (1986) 700.
[30] Z. Yang, Q. Lu, L. Li, The genesis of period-adding bursting without bursting-chaos in the Chay model, Chaos Solitons Fract. 27 (2006) 689.
[31] V.S.M. Piassi, A. Tufaile, J.C. Sartorelli, Period-adding bifurcations and chaos in a bubble column, Chaos 14 (2) (2004) 477.
[32] G. Tanaka, S. Murashige, K. Aihara, Bifurcation structures of period-adding phenomena in an ocean internal wave model, Int. J. Bifurcat. Chaos 13 (11) (2003) 3409.
[33] V. Avrutin, M. Schanz, S. Banerjee, Codimension-three bifurcations: explanation of the complex one-, two-, and three-dimensional bifurcation structures in nonsmooth maps, Phys. Rev. E. 75 (2007) 066205.
[34] C. Halse, M. Homer, M. di Bernardo, C-bifurcations and period-adding in one-dimensional piecewise-smooth maps, Chaos Solitons Fract. 18 (2003) 953.
[35] D. Dutta, J.K. Bhattacharjee, Period adding bifurcation in a logistic map with memory, Physica D 237 (2008) 3153.
[36] J. Guckenheimer, P.J. Holmes, Nonlinear Oscillations, Dynamical Systems, and Bifurcations of Vector Fields, Springer, New York, 1986.